



Ultrafast saturable absorption dynamics in hybrid graphene/Si 3 N 4 waveguides

Pierre Demongodin, Houssein El Dirani, Jérémy Lhuillier, Romain Crochemore, Malik Kemiche, Thomas Wood, Ségolène Callard, Pedro Rojo-Romeo, Corrado Sciancalepore, Christian Grillet, et al.

► To cite this version:

Pierre Demongodin, Houssein El Dirani, Jérémy Lhuillier, Romain Crochemore, Malik Kemiche, et al.. Ultrafast saturable absorption dynamics in hybrid graphene/Si 3 N 4 waveguides. *APL Photonics*, 2019, 4 (7), pp.076102. <10.1063/1.5094523>. <hal-02461174>

HAL Id: hal-02461174

<https://hal.science/hal-02461174v1>

Submitted on 7 Jan 2021

HAL is a multi-disciplinary open access archive for the deposit and dissemination of scientific research documents, whether they are published or not. The documents may come from teaching and research institutions in France or abroad, or from public or private research centers.

L'archive ouverte pluridisciplinaire **HAL**, est destinée au dépôt et à la diffusion de documents scientifiques de niveau recherche, publiés ou non, émanant des établissements d'enseignement et de recherche français ou étrangers, des laboratoires publics ou privés.











HAL Authorization

Ultrafast saturable absorption dynamics in hybrid graphene/Si₃N₄ waveguides

Cite as: APL Photonics **4**, 076102 (2019); <https://doi.org/10.1063/1.5094523>

Submitted: 03 March 2019 . Accepted: 17 June 2019 . Published Online: 18 July 2019

 Pierre Demongodin,  Houssein El Dirani,  Jérémy Lhuillier, Romain Crochemore,  Malik Kemiche,  Thomas Wood,  Ségolène Callard, Pedro Rojo-Romeo, Corrado Sciancalepore,  Christian Grillet, and  Christelle Monat

COLLECTIONS



This paper was selected as Featured



View Online



Export Citation



CrossMark

ARTICLES YOU MAY BE INTERESTED IN

[Brillouin optomechanics in nanophotonic structures](#)

APL Photonics **4**, 071101 (2019); <https://doi.org/10.1063/1.5088169>

[Nonlinear optics in carbon nanotube, graphene, and related 2D materials](#)

APL Photonics **4**, 034301 (2019); <https://doi.org/10.1063/1.5051796>

[Strong frequency conversion in heterogeneously integrated GaAs resonators](#)

APL Photonics **4**, 036103 (2019); <https://doi.org/10.1063/1.5065533>

APL Photonics

SPECIAL TOPIC: Coronavirus and Photonics

Submit Today!

Ultrafast saturable absorption dynamics in hybrid graphene/Si₃N₄ waveguides

Cite as: APL Photon. 4, 076102 (2019); doi: 10.1063/1.5094523

Submitted: 3 March 2019 • Accepted: 17 June 2019 •

Published Online: 18 July 2019



Pierre Demongodin,^{1,a)} Houssein El Dirani,² Jérémy Lhuillier,¹ Romain Crochemore,² Malik Kemiche,¹ Thomas Wood,¹ Ségolène Callard,¹ Pedro Rojo-Romeo,¹ Corrado Sciancalepore,² Christian Grillet,¹ and Christelle Monat¹

AFFILIATIONS

¹ Université de Lyon, Institut des Nanotechnologies de Lyon (INL) UMR 5270, École Centrale de Lyon, 69134 Écully, France

² Université Grenoble Alpes, CEA-LETI, Minatec, Optics and Photonics Division, 17 rue des Martyrs, F-38054 Grenoble, France

^{a)} Electronic mail: pierre.demongodin@ec-lyon.fr

ABSTRACT

We study the nonlinear optical properties of graphene integrated onto Si₃N₄ waveguides under picosecond and subpicosecond pulsed excitation at telecom wavelength. Saturable absorption of graphene under guided-mode excitation is measured, and the temporal effects related to the photoexcited carrier dynamics in graphene are highlighted. Thereafter, a model of photoexcited carriers in graphene is implemented into the nonlinear Schrödinger equation in order to simulate the pulse propagation across the hybrid graphene/Si₃N₄ waveguide. This allows us to extract phenomenological parameters of graphene saturable absorption in chip-based devices, which could provide some guidelines for the design of nonlinear elements in photonic integrated circuits.

© 2019 Author(s). All article content, except where otherwise noted, is licensed under a Creative Commons Attribution (CC BY) license (<http://creativecommons.org/licenses/by/4.0/>). <https://doi.org/10.1063/1.5094523>

1. INTRODUCTION

Over the past decade, graphene, a bi-dimensional lattice of carbon atoms, has generated plenty of interest for both fundamental and applied research in microelectronics and more recently in optoelectronics.^{1,2} Its unique properties,³ mostly related to the Dirac cone electronic dispersion,⁴ make it an outstanding material candidate for both electronic and photonic device applications.^{5–8} Among all relevant properties, the optical nonlinearity of graphene was pointed out to be much larger than those in traditional semiconductor and glass materials.^{9–11} In addition, this nonlinear response could be dynamically tuned through electrical gating,^{12–15} with the prospect of realizing fast, reconfigurable, and flexible nonlinear devices. Last but not least, the planar geometry of graphene makes it relatively easy to transfer this carbon layer onto photonic chips, as part of postprocessing techniques. Integrated optics can indeed bring what graphene lacks due to its atomic layer thickness, i.e., a way to reinforce the interaction between light and this 2D-material through the use of resonant or light-confining geometries. Graphene could thus lead to a new generation of nonlinear photonic devices and chips that combine the existing know-how

on integrated optics with graphene strong and tunable nonlinear properties.

On the one hand, several $\chi^{(3)}$ based nonlinear effects in graphene have been investigated theoretically^{9,10,16,17} and experimentally. Related measurements using either free-space excitation or interaction with guided light waves have demonstrated four-wave mixing,^{11,13,18–20} self-phase modulation,^{21–23} and third harmonic generation.^{24,25} However, all these works have reported a large disparity in the quantitative estimation of the third-order nonlinear refractive optical response.^{14,16} This issue remains still poorly understood and could be attributed to the different experimental conditions used to probe graphene, to the quality of graphene itself, or to the material environment in the vicinity of graphene. In particular, the unambiguous extraction of the nonlinear response of graphene is not straightforward when this 2D material is deposited on top of another nonlinear refractive material, like silicon, for instance.

On the other hand, graphene is known to act as a saturable absorber.^{26–28} This nonlinear signature has been widely used for the realization of passively mode-locked fiber lasers.^{29–34} Although

some theoretical papers attempted to model saturable absorption in graphene,^{26,27} the correlation with experimental studies is still imperfect.²⁷ More importantly, its implementation onto chip-based platforms remains elusive but could form the critical nonlinear element of either integrated mode-locked lasers or more generally advanced photonic integrated circuits, such as chip-based photonic neural networks and programmable nanophotonic processors.³⁵ So far, most studies have focused on either third-order nonlinear refractive processes or saturable absorption separately. However, these two effects are likely to occur under a similar regime of excitation, and their interplay cannot be ignored. Although not directly investigating the effect of saturable absorption, Vermeulen *et al.*²¹ recently pointed out that self-phase modulation in glass waveguides covered with graphene could be explained by the generation of free carriers in graphene and the related change in refractive index at the time scale of the picosecond pulse duration used in the experiment. This suggests that saturable absorption of graphene could have a non-negligible impact on third-order nonlinear refractive processes. Most importantly, the time scale of free carrier recombination in graphene, which is known to be much shorter (~ 1 ps) than in traditional semiconductor materials, might have important consequences on the dynamics and magnitude of these nonlinear effects. In Ref. 21, saturable absorption was not reported, possibly due to the low power regime (~ 2 W peak power) that was used. In addition, the effects of carrier dynamics, as dictated by the temporal pulse duration of the pump, were not fully investigated.

In this work, we demonstrate the signature of saturable absorption of graphene in chip-based platforms by measuring the transmission of near-infrared optical pulses in hybrid graphene/ Si_3N_4 waveguides. We take advantage of the relatively weak nonlinear properties of the underlying Si_3N_4 material for studying unambiguously graphene nonlinear properties. From our measurements across a large dynamic range of pulse peak power (from 0.2 W up to a few hundreds), we observe a substantial rise of the transmission by more than a factor 2, which increases with graphene interaction length. By varying the pulse duration from the picosecond to sub-picosecond, we also report a variation of the absorption saturation of graphene, thereby revealing some dynamics of this effect. We correlate these measurements with a nonlinear pulse propagation model taking into account graphene interaction length, the linear

and nonlinear response of the hybrid waveguide, power-dependent loss in graphene, and the associated dynamics of free carrier relaxation. These studies attempt to clarify the interplay between saturable absorption and third-order nonlinear refractive processes in graphene, which should help realize more efficient graphene based nonlinear devices on a chip.

II. GRAPHENE ON SILICON NITRIDE HYBRID DEVICES AND LINEAR MEASUREMENTS

The photonic chip used for the characterization of graphene nonlinear optical properties features 2 cm long Si_3N_4 waveguides buried in silica.^{36,37} The silica top cladding of the waveguides was removed using a perfectly selective chemical-mechanical planarization, so as to leave the waveguides top surface exposed in air with no Si_3N_4 consumption and no remaining topography. The cross section dimensions of the Si_3N_4 waveguides are $1.5 \mu\text{m} \times 0.66 \mu\text{m}$ (width \times height). Figure 1 displays the electric field intensity of the fundamental TE mode that will be excited in our experiments. Butt-coupling transmission measurements of a series of these unclad Si_3N_4 waveguides with different lengths allowed us to extract waveguide propagation losses of 3 dB/cm and coupling loss of around 4 dB per facet. The latter is lowered, thanks to the use of inverse tapers close to the chip input/output.

Trivial transfer graphene, purchased from ACS Materials®, was transferred onto the chip. The waveguide planarization step mentioned above allows us to take advantage of an increased interaction between the guided mode and graphene that lies directly on the surface of the waveguide. We also note that this geometry conveniently presents a planar surface that is ideal for the mechanical transfer of graphene. As shown in the optical microscope image of Fig. 2(a), the transfer provides us with a series of waveguides with a variable coverage of graphene. Four waveguides are available for study, with a graphene interaction length of 0.5, 1.4, 2.3, and 3.2 mm. An additional Si_3N_4 waveguide without graphene will be used as a reference.

Raman measurements were performed after the transfer, and a typical spectrum obtained in the vicinity of the waveguides of interest is shown in Fig. 2(b). The characteristics of this spectrum

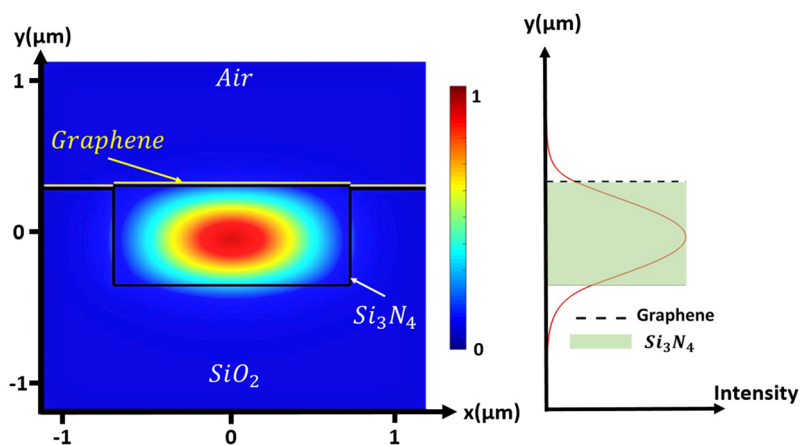


FIG. 1. Normalized electric field intensity of the fundamental TE mode of the graphene-covered Si_3N_4 waveguide and intensity of the electric field $|E_z|^2$ component in the plane of graphene along the y -axis at the center of the waveguide ($x = 0$).

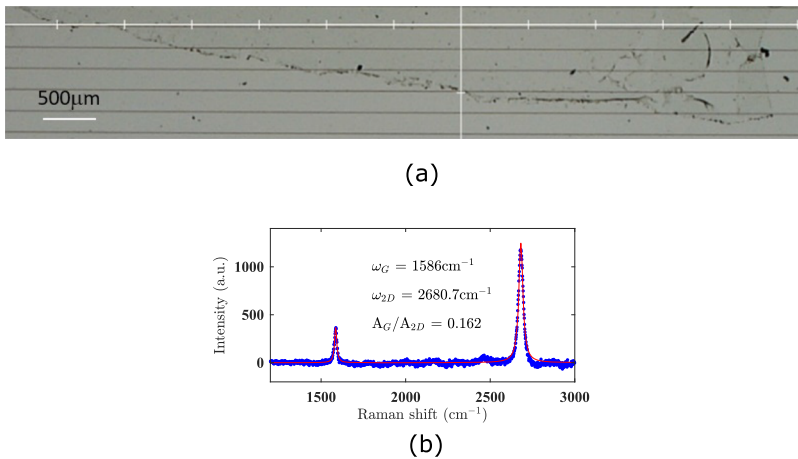


FIG. 2. (a) Optical microscope image of the graphene transferred onto Si_3N_4 optical waveguides. (b) Raman spectrum of the graphene covered chip. The A_G/A_{2D} ratio suggests that graphene has a monolayer thickness while the absence of D peak confirms the quality of graphene.

(the integrated intensity ratio of the G and 2D band, A_G/A_{2D} , in particular) confirm the presence of monolayer graphene.³⁸

Using a low power continuous-wave laser at 1540 nm coupled to the chip (with $\sim 30 \mu\text{W}$ power) in the TE-polarization, we characterize the linear response of the hybrid graphene/ Si_3N_4 waveguides. Figure 3(a) shows the total transmission of the waveguides as a function of the length of graphene that covers them. The coupling loss per facet is relatively unchanged with respect to that of the unclad Si_3N_4 waveguides, and the slope of the linear (dB scale) transmission allows us to infer an average propagation loss α_0 of 126 dB/cm induced by the presence of graphene. The good linear fit ($R^2 = 0.991$) of the transmission with graphene length seems to confirm the relatively homogeneous properties (at least at the millimeter scale) of graphene transferred onto the chip. In addition, the high optical losses of the graphene-covered waveguides attest the strong interaction between the mode and graphene. This loss figure is consistent with the overlap of graphene with the evanescent tail of the waveguide TE fundamental mode (around 0.013% of the intensity field, considering an effective thickness of 3.3 Å for graphene). The comparison of linear modal loss measurements of our hybrid waveguides across the wavelength range 1440 nm–1640 nm with simulations (Lumerical commercial software) allows us to extract a Fermi level of around -0.3 eV corresponding to an approximate p-doping of $9 \times 10^{12} \text{ cm}^{-2}$, which is expected for CVD graphene and this transfer process.³⁹ In Fig. 3(b), we plot the effective length calculated

through⁴⁰ $L_{\text{eff}} = \frac{1 - \exp^{-\alpha_0 L_{\text{gr}}}}{\alpha_0}$ as a function of the physical graphene interaction length L_{gr} varying between 0.5 mm and 3.5 mm. This curve gives an estimate of the waveguide length along which light effectively propagates before it gets fully absorbed. This effective length saturates beyond 1.5 mm graphene length due to the high linear propagation losses of the hybrid waveguide. This suggests that we might not observe much difference in terms of the related nonlinear signature when probing waveguides covered by graphene length beyond 1.5 mm.

III. NONLINEAR CHARACTERIZATION SETUP

For the study of the nonlinear properties of the graphene-covered waveguides, we use a fiber-based pulsed laser that delivers $\sim 2 \text{ ps}$ pulses at 1547 nm and with a repetition rate of 20 MHz. The setup is presented schematically in Fig. 4(a): it includes a polarizer so as to excite the TE mode of the chip and a variable optical attenuator to vary the pump power coupled to the waveguides using lensed fibers. 1% of the input power is tapped for monitoring the pump power coupled to the chip, while a coupler at the output allows us to measure both the spectrum (via an optical spectrum analyzer) and the power collected at the end of the waveguides (via a power meter).

To reach higher peak powers, we amplify the nearly Fourier-transform limited pulses from the laser using an Erbium Doped Fiber Amplifier (EDFA). The use of this EDFA gives us some

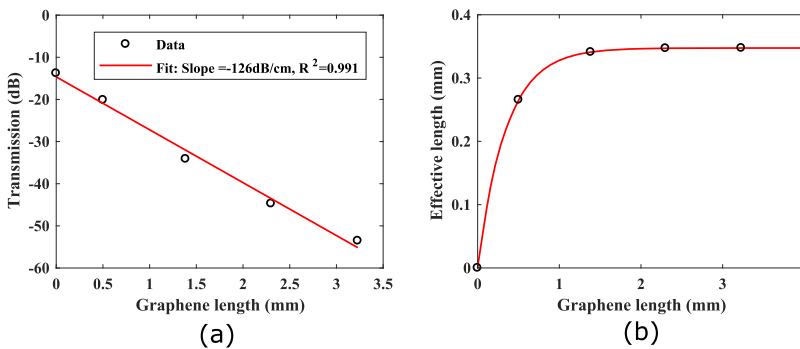


FIG. 3. (a) Measured waveguide transmission (circles) as a function of the interaction length with graphene. The red line is a linear fit associated with a slope of 126 dB/cm. (b) Effective length as a function of the graphene interaction length for $\alpha_0 = 126 \text{ dB/cm}$. The circles highlight the graphene lengths that are available on the sample.

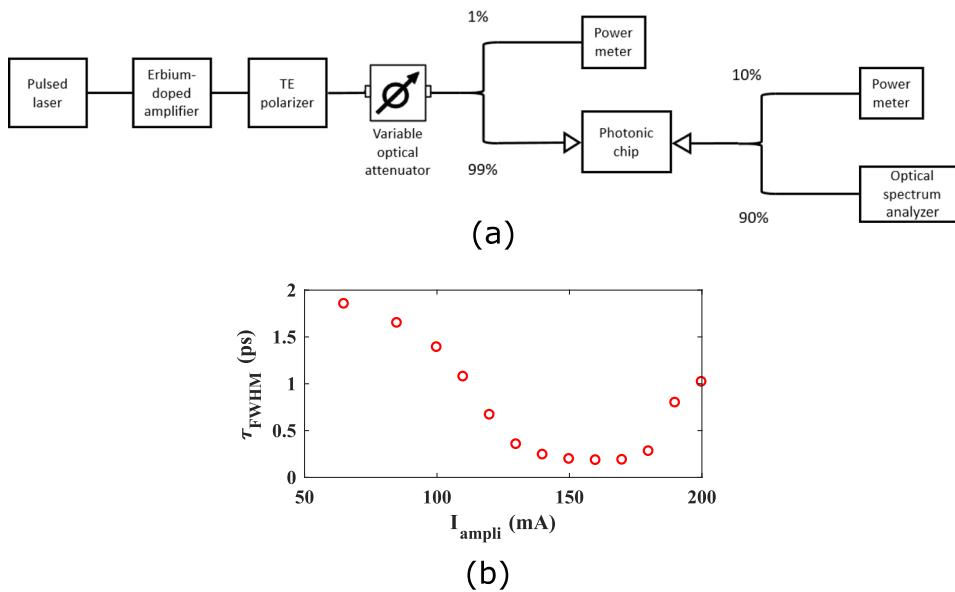


FIG. 4. (a) Fiber optic setup used for the measurements of the graphene covered Si_3N_4 waveguides in the nonlinear regime. (b) Relation between the input pulse duration (FWHM) at the entrance of the chip and the pump current of the amplifier, as measured with a commercial autocorrelator.

flexibility in terms of pulse duration, allowing us to investigate the dynamics of the graphene/ Si_3N_4 waveguide nonlinear response. For EDFA pump currents above a certain threshold (typically 85 mA in our setup), the amplified pulses are modified in both the spectral and temporal domains at the entrance of the chip. In particular, the combined effects of nonlinearity along the fiber (basically self-phase modulation) and its negative dispersion at 1547 nm induce some temporal compression of the pulse, depending on the amplified pulse peak power.

Practically, as we increase the EDFA pump current, the initially Fourier-transform limited pulse narrows in the temporal domain (for pump current up to ~ 160 mA) until a minimum temporal width is reached. For EDFA pump current above 160 mA, the pulse duration increases due to a gradual splintering of the pulse in the time domain. Therefore, it is possible to adjust the pulse duration by changing the EDFA pump current, while independently controlling the pump peak power (i.e., the pulse energy) coupled to the chip via the attenuator. Autocorrelation measurements of the input pulses close to the entrance of the chip were performed so as to provide an estimation of the input pulse duration. Figure 4(b) shows the relation between the inferred pulse duration and the EDFA pump current. Our autocorrelation measurements show variations of about one order of magnitude, from 2 ps (initial pulse duration at the output of the laser) down to 0.2 ps approximately. This additional degree of freedom via controlling the EDFA pump current allows us to investigate the dependence of the nonlinear effects on the pulse duration on the nonlinear effects occurring in the hybrid graphene/ Si_3N_4 waveguides.

IV. EXPERIMENTAL NONLINEAR RESULTS

We first present the nonlinear transmission of graphene/ Si_3N_4 waveguides when excited by subpicosecond pulses at 1547 nm with increasing peak power and a fixed pulse duration (~ 0.2 ps, for an EDFA pump current of 160 mA). Figure 5 shows the waveguide

transmission as a function of the coupled pulse energy, ranging between 0.15 and 150 pJ (i.e., 0.6–600 W coupled peak power), for the series of waveguides covered with different graphene lengths. Figure 5(a) exhibits the absolute transmission of the waveguides, whereas Fig. 5(b) displays the normalized transmission, i.e., divided by the transmission at low energy ($E_{\text{pulse}} = 3$ pJ) for each waveguide. Figure 5(b) thus allows us to appreciate and compare the relative variation in transmission for the waveguides covered by different graphene lengths (between 0.5 mm and 3.2 mm), along with the reference waveguide (darkest blue) without graphene.

As a first observation, the transmission increases with pulse energy whenever graphene is present, while the reference curve (without graphene) remains flat, thereby confirming that the rise in transmission is related to graphene. Second, the rise in transmission is somewhat correlated with the graphene interaction length, at least between 0 mm, 0.5 mm, and the three other lengths. We attribute these observations to the saturable absorption of graphene. We highlight that this signature is not hidden here by other kinds of nonlinear absorption loss that might otherwise occur at these power levels in the underlying waveguide such as, for instance, in silicon waveguides.

In the case of $L_{\text{gr}} = 0.5$ mm [lightest blue in Fig. 5(b)], the measured increase in transmission rolls off above 100 pJ. We explain this clamping behavior by a nonsaturable absorption component of graphene, as the maximum transmission value (-20 dB) remains well below that of the waveguide without graphene (-14 dB) as observed in Fig. 5(a).

For graphene lengths between 1.4 mm and 3.2 mm, the transmission continuously increases with pulse energy by more than a factor two with respect to the low power transmission. The similar signature observed for the three longest graphene/ Si_3N_4 waveguide is somewhat expected due to the saturation of the effective length (considering the hybrid waveguide propagation loss) beyond 1.5 mm of graphene length, which reaches a constant value of around $L_{\text{eff}}^{\text{max}} = 0.345$ mm. Qualitatively, once the effective length

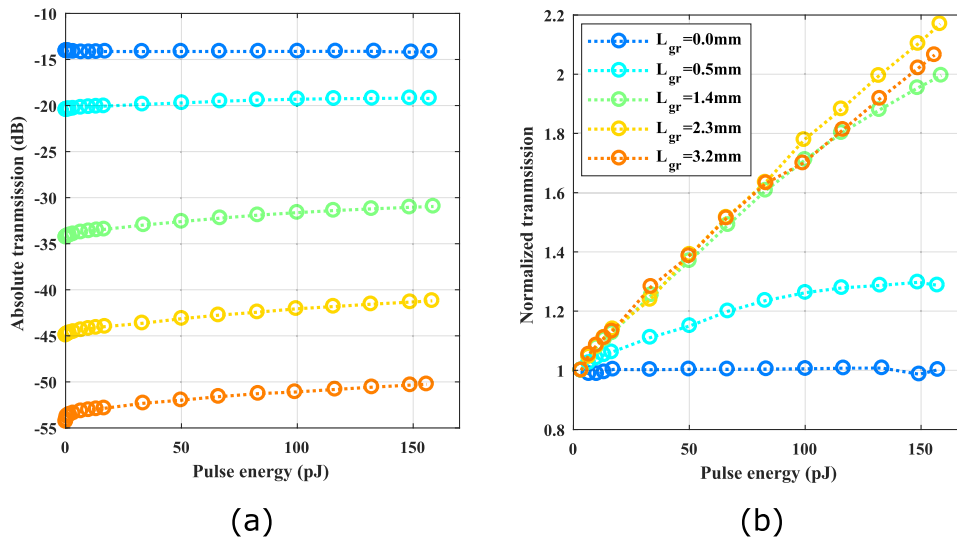


FIG. 5. (a) Absolute transmission as a function of the coupled pulse energy ($I_{\text{ampli}} = 160$ mA, $\tau_{\text{FWHM}} = 0.2$ ps, 20 MHz, 1547 nm) for Si_3N_4 waveguides covered by different graphene lengths. (b) Related normalized transmission for the same series of waveguides, where each transmission curve is normalized by the corresponding transmission at low pulse energy ($E_{\text{pulse}} = 3$ pJ).

is reached (at ~ 1.5 mm propagation distance), the pulse energy becomes too weak to induce any absorption saturation in the remaining section of graphene further in the waveguide. From our experimental results, we can thus conclude that graphene absorption saturation almost exclusively occurs in the first millimeter and half of our hybrid waveguides under the probed range of pulse energies.

Next, we investigate the effect of pulse duration on the saturation of graphene absorption, by varying the pump current of the EDFA, while controlling the average power (i.e., the pulse energy) coupled to the waveguide using the variable optical attenuator. As already explained, the pump current of the EDFA affects the pulse shape and duration, i.e., the temporal distribution of pump photons, while the attenuator sets the pulse energy, i.e., the number of photons comprised in the pulse. We can therefore control the pulse energy and duration relatively independently. However, the range of pulse duration that can be investigated for higher pulse energies is restricted by the high amplification gain requirements, as provided by the EDFA under higher pump currents. This leads to a narrower range of (short) pulse duration that can be probed for higher pulse energies.

In order to study how the pulse duration impacts saturable absorption of graphene, we measure the waveguide transmission while varying the EDFA pump current (i.e., pulse duration) for a fixed pulse energy. We thus only change how photons are temporally distributed but not their number. Figure 6 shows the results of these measurements. We plot the transmission (normalized with respect to the low pulse energy transmission at the lowest EDFA pump current setting) as a function of the EDFA pump current, with different colors used for different values of coupled pulse energy (between 0.3 pJ and 148.8 pJ). The results are shown for three hybrid graphene/ Si_3N_4 waveguides covered with 0.5 mm [Fig. 6(a)], 1.4 mm [Fig. 6(b)], and 2.3 mm [Fig. 6(c)] graphene lengths. To re-emphasize the link between the EDFA pump current and the pulse duration, we also present in Fig. 6(d) the related normalized transmission vs the pulse duration inferred from these measurements for the case $L_{gr} = 2.3$ mm and EDFA pump current below 170 mA.

First, we notice a global increase in the transmission with the pulse energy at all EDFA pump currents, which corroborates the absorption saturation results from Fig. 5, independently of the pulse duration. Next, we see that for a fixed pulse energy (one colored curve in Fig. 6), the normalized transmission increases with decreasing pulse duration, with a maximum obtained around 160 mA EDFA current corresponding to the shortest pulses. This behavior is more striking for higher pulse energies, while at low values of 0.3 pJ and 1.7 pJ, the increase in transmission is very weak due to the limited amount of saturable absorption.

These results suggest that temporal effects occur at the pulse time scale, while the pulse propagates through the hybrid graphene/ Si_3N_4 waveguide, related to the free carrier excitation and relaxation dynamics in graphene. We model these effects in Sec. V, so as to extract some phenomenological parameters describing the dynamics of absorption in graphene and its impact on the nonlinear propagation of picosecond pulses.

V. MODEL AND DISCUSSION

To simulate the pulse propagation in nonlinear waveguides, we use the nonlinear Schrödinger equation (NLSE),⁴⁰ in the slowly varying envelope approximation, and numerically solve it using the Split-Step Fourier Method (SSFM). This equation allows us to calculate the pulse envelope $A(z, T)$ of the electric field according to

$$\frac{\partial A}{\partial z} + i\frac{\beta_2}{2}\frac{\partial^2 A}{\partial T^2} = -\frac{\alpha(N_c)}{2}A + i\gamma|A|^2A. \quad (1)$$

In this equation, β_2 is the second-order dispersion of the waveguide, the waveguide propagation loss is dominated by $\alpha(N_c)$, which is the carrier density dependent absorption of graphene, and the nonlinear parameter γ takes into account the effective area of the mode profile A_{eff} and the effective nonlinear Kerr index of the waveguide n_2 . Two-photon absorption can be readily implemented in this equation (as a positive imaginary part of γ), but we did not include it here because the graphene induced linear absorption dominates the waveguide loss at all powers, whereas the Si_3N_4 material

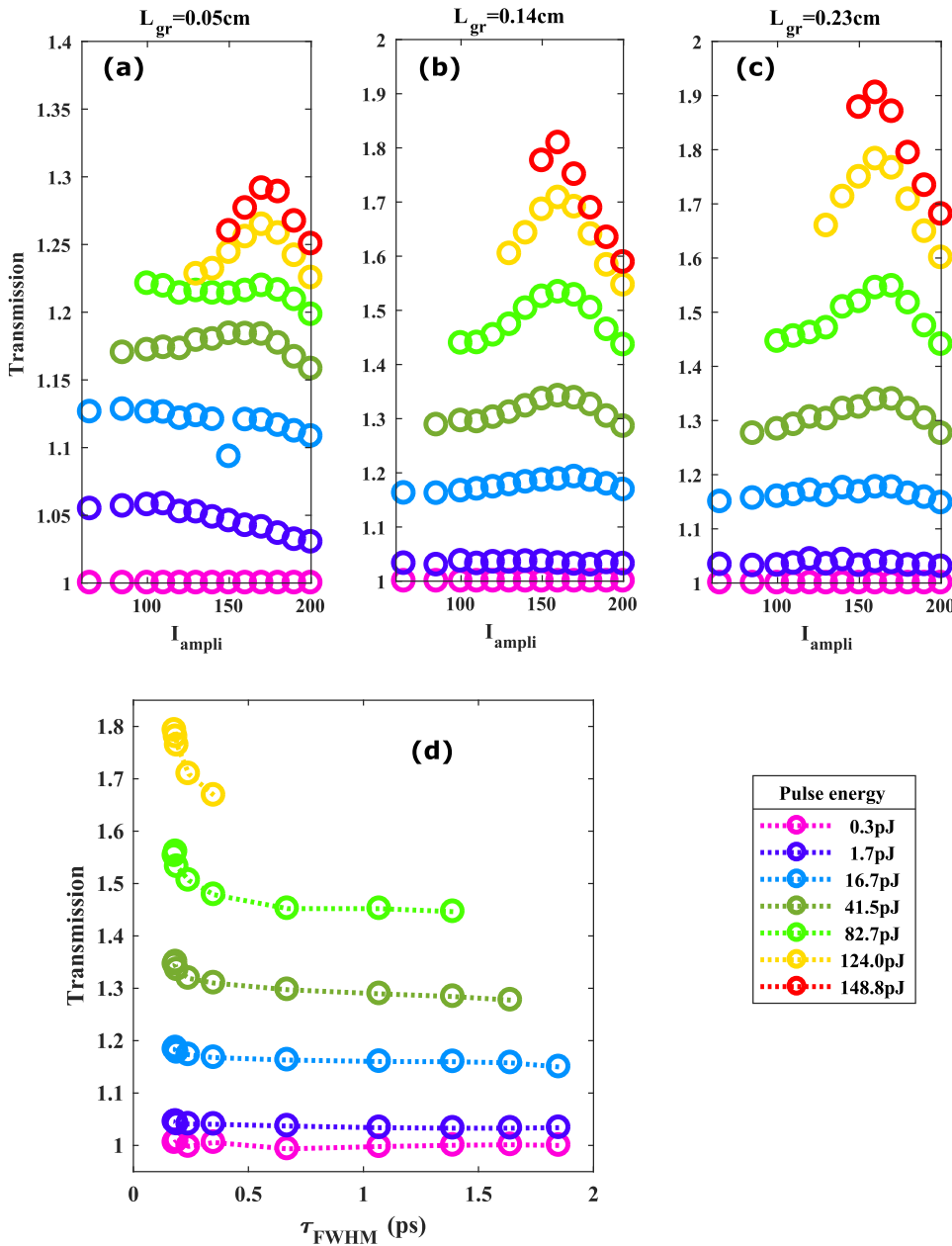


FIG. 6. Normalized transmission as a function of the EDFA pump current I_{ampli} (mA) for waveguides covered by graphene lengths of 0.5 mm (a), 1.4 mm (b), and 2.3 mm (c). The low power transmission (at 0.3 pJ coupled pulse energy, $I_{\text{ampli}} = 65$ mA) is used for the transmission normalization. On each plot, the different colors correspond to different values of coupled pulse energy between 0.3 pJ and 148.8 pJ. (d) Normalized transmission as a function of the pulse duration for different pulse energies and $L_{\text{gr}} = 2.3$ mm ($I_{\text{ampli}} < 170$ mA).

does not exhibit two-photon absorption at telecom wavelengths due to its high bandgap energy.

This equation allows us to simulate both the spectral and temporal signature of the pulse upon its propagation in the waveguide, while taking into account all kinds of linear and nonlinear effects that might interact and impact the pulse evolution. We use it here essentially to clarify the measured variation in the transmission upon increasing pulse energy and the impact of the pulse temporal characteristics on the graphene/Si₃N₄ hybrid waveguide transmission.

We do not account for the graphene saturable absorption in Eq. (1) as a perturbative process that might be included in the imaginary part of $\chi^{(3)}$, i.e., as an intensity dependent imaginary contribution to the nonlinear parameter γ . Instead, we describe it through the $\alpha(N_c)$ absorption dependence on the surface carrier density in graphene lying on top of the waveguide. First, we consider both a saturable and a nonsaturable part of graphene absorption, as suggested by our experimental results, via

$$\alpha(N_c) = \alpha_{\text{NS}} + \alpha_{\text{sat}} \left(1 - \frac{N_c}{N_{\text{sat}}} \right). \quad (2)$$

At low power, the sum of α_{NS} and α_{sat} is equal to the measured waveguide graphene induced absorption loss α_0 , i.e., 126 dB/cm. As widely acknowledged, the saturable part of graphene absorption α_{sat} is mostly caused by Pauli blocking in the Dirac cone dispersion of graphene, allowing for interband transitions only if the excited state is empty.³⁰ One phenomenological way to describe this is to consider a simple system with two energy bands between which the transition probability is directly linked to the carrier occupation of the upper band, i.e., to the excited carrier surface density N_c in the upper band. The temporal evolution of N_c in graphene can then be described by Eq. (3), which is adapted from the corresponding equation in the work of Vermeulen *et al.*,²¹

$$\frac{\partial N_c}{\partial t} = \frac{\alpha_{sat}}{\hbar\omega} \left(1 - \frac{N_c}{N_{sat}}\right) \frac{|A|^2}{w} - \frac{N_c}{\tau_c}. \quad (3)$$

The inclusion of the waveguide width w in this equation explicitly accounts for the effect of the lateral confinement of the waveguide, which restricts the interaction of light with graphene, as mediated by the waveguide mode, across a limited dimension (equal to w). A decrease in the waveguide width thus directly translates into the reduction of the launched power necessary to saturate graphene absorption. In Eqs. (2) and (3), N_{sat} represents the saturated excited carrier density per unit of graphene surface area upon which the saturable fraction of graphene absorption is forbidden due to Pauli blocking. The use of the factor $\left(1 - \frac{N_c}{N_{sat}}\right)$ conveys the idea that the probability to absorb a photon via an interband process, hence the creation of a photoexcited carrier in the conduction band, depends on the filling of the upper level considered, i.e., on the excited carrier density N_c . By including the sole contribution of α_{sat} in Eq. (3) as responsible for carrier generation in graphene, we assume that only the saturable absorption part of graphene is conducive to fill in the conduction band at the photon energy level considered. We indeed relate the coefficient α_{NS} to other absorption processes caused, for instance, by a nonideal graphene, or some residual polymer layer on top of graphene or to other additional absorption loss contribution processes that will not generate carriers. These should not, *a priori*, contribute to the generation of carriers at the energy allowing Pauli blocking to occur. In Eq. (3), τ_c is a phenomenological lifetime accounting for the different processes that may lead to

the relaxation and recombination of excited carriers in graphene. The set of equations (1)–(3) allows us to compute the pulsed signal at the output for different values of input pulse energy and duration.

To compare our simulations with the measurements presented in Fig. 6, we first need to model the pulsed signal experimentally sent at the entrance of the waveguide. Our autocorrelation and spectral measurements of the input signal enable us to reconstruct our experimental input pulses. Indeed, the temporal and spectral shapes of the input pulses directly result from the combined effects of self-phase modulation and dispersion upon propagation in a several meter long fiber (associated with both the EDFA and the fiber used to couple to the chip) with anomalous dispersion. We can thus numerically emulate the input pulses to be used in our simulations so that they resemble the experimental input pulses (see [supplementary material](#), Sec. I). For this, we use the split step Fourier method so as to simulate, in a way somewhat equivalent to what happens in our setup, the propagation of a 2 ps Fourier Transform limited sech^2 pulse of given peak power P_{peak} into a 10 m long link of fiber with standard values of nonlinear parameter γ and anomalous dispersion.

To have a quantity equivalent to the experimental EDFA pump current setting, we then just adapt the numerical value of P_{peak} so that the simulated “input” pulse characteristics match both the spectrum and autocorrelation measurements of the input pulses at the entrance of the waveguide, for each EDFA current (see [supplementary material](#), Sec. I for related plots). Once the input pulse shape is so determined, we can vary the pulse energy independently in our simulations. This numerically tailored input signal is next propagated into the hybrid graphene/Si₃N₄ chip by solving the set of equations (1)–(3), so as to reproduce the different curves of Fig. 6.

We plot in Fig. 7 the results of these simulations (solid lines), by using the model parameter values indicated in Table I for the three hybrid waveguides and for various values of coupled pulse energies along with the experimental data (circles) from Fig. 6.

Our model allows us to reproduce the general trend experimentally observed in Fig. 6, namely, the slight rise of transmission measured for decreasing pulse duration (achieved around $I_{ampli} = 160$ mA) at a fixed pulse energy coupled to the waveguides.

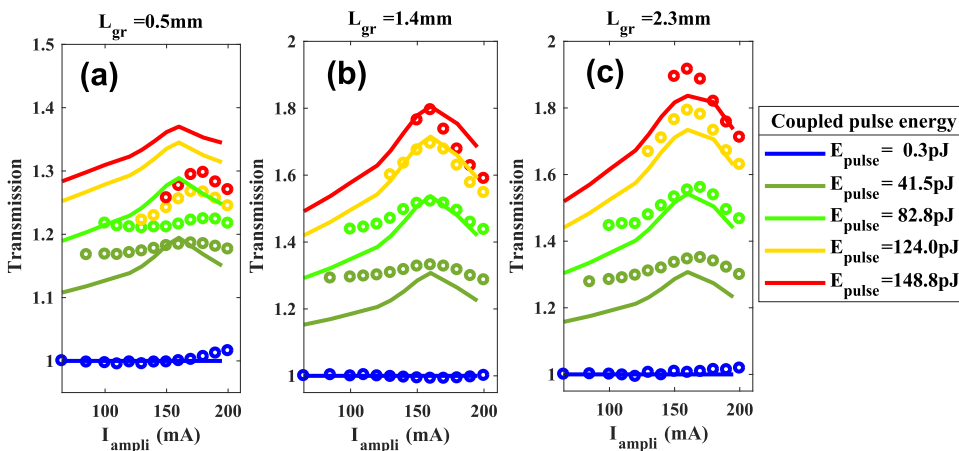


FIG. 7. Normalized pulse transmission from simulations (solid lines) and experiments (circles) as a function of the EDFA pump current, effectively related to a variable input pulse duration for the three hybrid graphene/Si₃N₄ waveguides. For each plot with a graphene length of 0.5 mm (a), 1.4 mm (b), and 2.3 mm (c), the different colors correspond to different values of coupled pulse energies. The parameters used for the simulation are given in Table I.

TABLE I. Values of the parameters used in the simulations.

A_{eff}	n_2	β_2	N_{sat}	τ_c	α_{NS}	α_0
$0.81 \mu\text{m}^2$	$2.6 \times 10^{-19} \text{ m}^2 \text{ W}^{-1}$	$-9.15 \times 10^{-26} \text{ s}^2 \text{ m}^{-1}$	$1.3 \times 10^{16} \text{ m}^{-2}$	150 fs	$0.6 \times \alpha_0$	126 dB/cm

For both $L_{gr} = 1.4 \text{ mm}$ and $L_{gr} = 2.3 \text{ mm}$, the change in transmission induced by the temporal distribution of pump photons is well accounted for by our model, especially for the highest coupled pulse energies, where the relative transmission with respect to the low power transmission increase is maximum ($\sim 190\%$). Indeed, for these two lengths, we manage to get a good agreement for both the absolute increase in the normalized transmission and also its variation with pulse duration. For lower pulse energy, the simulations tend to slightly underestimate the rise in transmission that is experimentally observed. This could be explained by a slight variation of the input pulse characteristics for low values of pulse energy. For the case $L_{gr} = 0.5 \text{ mm}$, the simulations overestimate the rise in transmission at the two highest pulse energies and fail to predict the saturation in the rise of transmission observed in this case. Some possible explanation for this deviation could be related to some defects close to the edge of the transferred graphene area (where this waveguide with $L_{gr} = 0.5 \text{ mm}$ is located), which might induce a larger contribution of α_{NS} .

The different parameters extracted from the comparison between the measurements and the simulations are mostly phenomenological, as is our model. But they could be useful for the design of nonlinear graphene-based devices. Most importantly, they describe average quantities across a wide area of graphene, instead of local measures that are more likely subjected to variations depending on the particular graphene quality and inhomogeneity.

The surface carrier density (in the graphene layer part that covers the waveguides) necessary to saturate graphene absorption and which best fits with our results N_{sat} is equal to $1.3 \times 10^{16} \text{ m}^{-2}$. It is comparable to the values previously reported in the literature (for example, $\sim 10^{17} \text{ m}^{-2}$ according to Bao *et al.*³³) and is consistent with the density of states in graphene at $D(\frac{\hbar\omega}{2} \approx 0.4 \text{ eV}) \sim 6 \times 10^{16} \text{ m}^{-2}$.

In our structures, we find that 60% of graphene absorption is not saturable. Based on our low power graphene absorption value of $\alpha_0 = 126 \text{ dB/cm}$, graphene losses along our hybrid waveguides may thus be reduced down to $\alpha_{NS} = 75 \text{ dB/cm}$. In our experiment and for $L_{gr} = 1.4 \text{ mm}$, the transmission doubles for the highest pulse energy. This corresponds to an average loss of $\alpha = 105 \text{ dB/cm}$ along the hybrid graphene/Si₃N₄ structure at high peak power ($\sim 600 \text{ W}$). Although the physical origin of a nonsaturable component of absorption in graphene is still poorly understood,²⁷ the quality of graphene and possibly the presence of graphene edges seem to play an important role. Moreover, it is very likely that thermal effects occur, as the coupled mean power (up to $\sim 3 \text{ mW}$ for highest pulse energy) is relatively high, and the energy mostly absorbed across a short distance of graphene. On a faster scale, the phenomenological relaxation time does not allow us to fully describe the dynamics of hot, photoexcited carriers in graphene. Finally, more complex effects such as two photon absorption, refraction, and absorption caused by free carriers generated in graphene could contribute indirectly to the emergence of an effective

nonsaturable component of the absorption that appears for short graphene lengths.

In our model, the saturable absorption is directly explained by Pauli blocking, related to the filling state of the upper band. From the comparison of our simulations and experiments, we retrieve a corresponding phenomenological lifetime $\tau_c = 150 \text{ fs}$ for the excited carriers. This lifetime accounts for all kinds of relaxation and recombination processes that might occur in graphene and indicates how much time a given photoexcited carrier stays, on average, in the excited state so as to forbid subsequent carrier excitation into the upper band. This lifetime effectively takes into account both intraband and interband relaxation processes that enable photoexcited carriers to leave the upper state filled upon the absorption of pump photons. As for N_{sat} , this parameter most likely depends on our photon excitation wavelength ($\hbar\omega = 0.8 \text{ eV}$) and the initial doping of graphene.

Previous nonlinear studies on hybrid graphene based waveguides have focused on the third-order refractive nonlinear response of graphene, without much attention paid to the saturable absorption, possibly due to the lower power regimes under investigation ($P_{peak} \leq 2 \text{ W}$). Here, we should be able to extract the nonlinear refractive signature as well, through measuring the spectral broadening of the pulses at the output of the waveguides, as caused by $\chi^{(3)}$ induced self-phase modulation. However, spectral broadening measurements of the output pulses, with or without graphene, provided very similar results in our case. The spectral changes caused by graphene were too small to extract any reliable value for the effective third-order nonlinear refractive index of graphene. This is strikingly different from what has been observed in the literature recently^{13,22,41} and all the more surprising as the range of pulse peak power probed in our work is much larger (by a factor 100 or more) than in previous studies. If we consider some estimated value for the graphene nonlinear coefficient of $n_2^{graphene} \sim -10^{-13} \text{ m}^2/\text{W}$ extracted from the literature,^{11,22} the effective coefficient of our hybrid graphene/Si₃N₄ waveguide should be roughly equal to $n_{2,eff}^{hybrid} \sim -10^{-17} \text{ m}^2/\text{W}$. According to our simulations, such a high effective negative third order nonlinear index of the hybrid graphene/Si₃N₄ would not necessarily cause a very strong spectral change, mostly due to the chirp of the excitation pulses at the entrance of the hybrid waveguide. However, the effect should still be noticeable on the spectrum and was not experimentally (see further discussion in [supplementary material](#), Sec. II). We alternatively implemented, in our model, the approach proposed by Vermeulen *et al.*,²¹ which considers the free carrier refraction in graphene instead of a nonlinear Kerr coefficient. The results are not really conclusive for the chirped input pulses considered here (see [supplementary material](#), Sec. II). Eventually, the spectral signature of the hybrid waveguide is better reproduced numerically through assuming a low refractive third-order nonlinear response of graphene, whether it be described through a Kerr

index nonlinear coefficient or a free-carrier refraction effect. The reason why we did not observe any strong self-phase modulation signature is still an open question. The residual graphene doping level could be partly responsible for this, as the optical response of graphene, including its nonlinear response, has been shown to strongly depend on the doping level.⁴²

We stress again that the most striking effect that was experimentally observed was the saturable absorption of graphene, which is fully accounted for by our model. We note that the consistent variation in transmission found by our simulations does not depend much on the nonlinear refractive response of our hybrid graphene/Si₃N₄ waveguide and under our experimental conditions. Considering the parameters used for graphene saturable absorption (α_{NS} , N_{sat} , and τ_c in Table I), the simulated transmission values are indeed similar for an effective nonlinear refractive index equal to either that of Si₃N₄ ($n_2^{Si_3N_4} = 2.6 \times 10^{-19} \text{ m}^2/\text{W}$) or that of a strongly nonlinear hybrid structure ($n_{2,eff}^{hybrid} = -10^{-17} \text{ m}^2/\text{W}$). Indeed, the pulse spectrum that is affected by the nonlinear refractive response has no direct impact on the saturable absorption since absorption is independent of wavelength in our model. This is a fair assumption considering the graphene optical response and the limited pulse spectrum span. As to potential spectral/temporal crossed effects, we note that the dispersion of our hybrid waveguides is very weak (the dispersion length $L_D \sim 14 \text{ cm}$ for the shortest pulses). Under these conditions, any change in the pulse spectrum along the waveguide does not have much effect on the temporal shape of the pulse, which predominantly impacts saturable absorption in our simulation. Hence, we can conclude that saturable absorption and refractive third-order nonlinear effects are relatively independent in our hybrid graphene/Si₃N₄ waveguide, although the conclusion might be strongly different for structures with higher dispersion.

Finally, our model allows us to take into account a wide range of $\chi^{(3)}$ based nonlinear effects as well as graphene saturable absorption and to investigate their interplay on the propagation of short optical pulses in hybrid nonlinear waveguides. Its relatively good agreement with our experimental results tends to demonstrate its validity, with carrier dynamics playing a central role in the observed rise in transmission. We re-emphasize that this model could be readily extended to include other kinds of phenomena such as free carrier induced absorption and refraction effects, if applicable.

VI. CONCLUSION

In conclusion, we studied the nonlinear optical response of graphene integrated onto Si₃N₄ waveguides under picosecond pulse excitation. The relatively weak nonlinear response of the underlying Si₃N₄ material allowed us to investigate and unambiguously isolate the nonlinear response of graphene for a much wider range of peak powers (up to a few hundred watts) than in previous work. Our results demonstrate a significant saturable absorption of graphene on a chip-based platform, which might provide a key nonlinear element for integrated mode-locked lasers or, more generally, advanced photonic integrated circuits such as programmable nanophotonic processors and optical neural networks. Furthermore, we showed a strong impact of the pulse duration (between 0.2 ps and 2 ps) onto the saturation of graphene absorption. We correlated these observations with a phenomenological model taking into account carrier

dynamics in graphene. By implementing this model in the nonlinear Schrödinger equation, we simulated the propagation of the optical pulses along hybrid graphene/Si₃N₄ waveguides, while including all effects related to waveguide dispersion, Kerr nonlinearity, and power dependent propagation loss in graphene. Our simulation results reproduce relatively well the experimentally measured power dependent variations in waveguide transmission. They also account for the impact of the pulse duration on this saturable absorption effect, which is effectively caused by carrier dynamics in graphene. The phenomenological parameters (saturated carrier density and carrier relaxation time) extracted from our model are consistent with values found for graphene in the literature. This re-emphasizes that carrier dynamics plays a central role in the nonlinear signature (here saturable absorption) of graphene in chip-based platforms. Finally, our model gives a comprehensive approach that can simulate the impact and interplay of various linear and nonlinear effects on the spectral and power variation of pulses propagating in nonlinear waveguides. As such, it represents a useful tool for unraveling the rich nonlinear response of hybrid graphene based waveguides, while providing guidelines for the design of efficient graphene chip-based devices.

SUPPLEMENTARY MATERIAL

See [supplementary material](#) for more information about input pulse characterization and modelization, as well as further discussion on spectral broadening measurements.

ACKNOWLEDGMENTS

This project has received funding from the European Research Council (ERC) under the European Union's Horizon 2020 research and innovation programme (GRAPHICS, grant agreement No. 648546).

REFERENCES

- ¹A. K. Geim and K. S. Novoselov, "The rise of graphene," *Nat. Mater.* **6**, 183–191 (2007).
- ²K. S. Novoselov, V. I. Fal'ko, L. Colombo, P. R. Gellert, M. G. Schwab, and K. Kim, "A roadmap for graphene," *Nature* **490**, 192–200 (2012); e-print [arXiv:0802.2267](#).
- ³A. H. Castro Neto, F. Guinea, N. M. R. Peres, K. S. Novoselov, and A. K. Geim, "The electronic properties of graphene," *Rev. Mod. Phys.* **81**, 109–162 (2009); e-print [arXiv:0709.1163](#).
- ⁴K. S. Novoselov, A. K. Geim, S. V. Morozov, D. Jiang, M. I. Katsnelson, I. V. Grigorieva, S. V. Dubonos, and A. A. Firsov, "Two-dimensional gas of massless Dirac fermions in graphene," *Nature* **438**, 197–200 (2005); e-print [arXiv:0509330 \[cond-mat\]](#).
- ⁵P. Avouris, "Graphene: Electronic and photonic properties and devices," *Nano Lett.* **10**, 4285–4294 (2010).
- ⁶Q. Bao and K. P. Loh, "Graphene photonics, plasmonics, and broadband optoelectronic devices," *ACS Nano* **6**, 3677–3694 (2012).
- ⁷F. Bonaccorso, Z. Sun, T. Hasan, and A. C. Ferrari, "Graphene photonics and optoelectronics," *Nat. Photonics* **4**, 611–622 (2010); e-print [arXiv:1006.4854](#).
- ⁸K. Kim, J. Y. Choi, T. Kim, S. H. Cho, and H. J. Chung, "A role for graphene in silicon-based semiconductor devices," *Nature* **479**, 338–344 (2011); e-print [arXiv:1205.4050](#).
- ⁹S. A. Mikhailov, "Non-linear electromagnetic response of graphene," *Europhys. Lett.* **79**, 27002 (2007); e-print [arXiv:0704.1909](#).
- ¹⁰J. L. Cheng, N. Vermeulen, and J. E. Sipe, "Third order optical nonlinearity of graphene," *New J. Phys.* **16**, 053014 (2014); e-print [arXiv:1609.06413](#).

- ¹¹E. Hendry, P. J. Hale, J. Moger, A. K. Savchenko, and S. A. Mikhailov, "Coherent nonlinear optical response of graphene," *Phys. Rev. Lett.* **105**, 097401 (2010); e-print [arXiv:0912.5321](#).
- ¹²B. Yao, S.-W. Huang, Y. Liu, A. K. Vinod, C. Choi, M. Hoff, Y. Li, M. Yu, Z. Feng, D.-L. Kwong, Y. Huang, Y. Rao, X. Duan, and C. W. Wong, "Gate-tunable frequency combs in graphene-nitride microresonators," *Nature* **558**, 410–414 (2018).
- ¹³K. Alexander, N. A. Savostianova, S. A. Mikhailov, B. Kuyken, and D. Van Thourhout, "Electrically tunable optical nonlinearities in graphene-covered SiN waveguides characterized by four-wave mixing," *ACS Photonics* **4**, 3039–3044 (2017); e-print [arXiv:1704.08567](#).
- ¹⁴T. Jiang, D. Huang, J. Cheng, X. Fan, Z. Zhang, Y. Shan, Y. Yi, Y. Dai, L. Shi, K. Liu, C. Zeng, J. Zi, J. E. Sipe, Y. R. Shen, W. T. Liu, and S. Wu, "Gate-tunable third-order nonlinear optical response of massless Dirac fermions in graphene," *Nat. Photonics* **12**, 430–436 (2018).
- ¹⁵G. Soavi, G. Wang, H. Rostami, D. G. Purdie, D. De Fazio, T. Ma, B. Luo, J. Wang, A. K. Ott, D. Yoon, S. A. Bourelle, J. E. Muench, I. Goykhman, S. Dal Conte, M. Celebrano, A. Tomadin, M. Polini, G. Cerullo, and A. C. Ferrari, "Broadband, electrically tunable third-harmonic generation in graphene," *Nat. Nanotechnol.* **13**, 583–588 (2018).
- ¹⁶N. A. Savostianova and S. A. Mikhailov, "Optical Kerr effect in graphene: Theoretical analysis of the optical heterodyne detection technique," *Phys. Rev. B* **97**, 165424 (2018).
- ¹⁷S. A. Mikhailov, "Theory of the nonlinear optical frequency mixing effect in graphene," *Physica E* **44**, 924–927 (2012).
- ¹⁸T. Gu, H. Zhou, J. F. McMillan, N. Petrone, A. Van Der Zande, J. C. Hone, M. Yu, G. Q. Lo, D. L. Kwong, and C. W. Wong, "Coherent four-wave mixing on hybrid graphene-silicon photonic crystals," *IEEE J. Sel. Top. Quantum Electron.* **20**, 116 (2014).
- ¹⁹M. Ji, H. Cai, L. Deng, Y. Huang, Q. Huang, J. Xia, Z. Li, J. Yu, and Y. Wang, "Enhanced parametric frequency conversion in a compact silicon-graphene microring resonator," *Opt. Express* **23**, 18679–18685 (2015).
- ²⁰T. Gu, N. Petrone, J. F. McMillan, A. van der Zande, M. Yu, G. Q. Lo, D. L. Kwong, J. Hone, and C. W. Wong, "Regenerative oscillation and four-wave mixing in graphene optoelectronics," *Nat. Photonics* **6**, 554–559 (2012); e-print [arXiv:1205.4333](#).
- ²¹N. Vermeulen, D. Castelló-Lurbe, M. Khoder, I. Pasternak, A. Krajewska, T. Ciuk, J. Cheng, H. Thienpont, and J. Van Erps, "Graphene's nonlinear-optical physics revealed through exponentially growing self-phase modulation," *Nat. Commun.* **9**, 2675 (2018).
- ²²N. Vermeulen, D. Castelló-Lurbe, J. Cheng, I. Pasternak, A. Krajewska, T. Ciuk, W. Strupinski, H. Thienpont, and J. Van Erps, "Negative Kerr nonlinearity of graphene as seen via chirped-pulse-pumped self-phase modulation," *Phys. Rev. Appl.* **6**, 044006 (2016).
- ²³A. Ishizawa, R. Kou, T. Goto, T. Tsuchizawa, N. Matsuda, K. Hitachi, T. Nishikawa, K. Yamada, T. Sogawa, and H. Gotoh, "Optical nonlinearity enhancement with graphene-decorated silicon waveguides," *Sci. Rep.* **7**, 45520 (2017).
- ²⁴N. Kumar, J. Kumar, C. Gerstenkorn, R. Wang, H. Y. Chiu, A. L. Smirl, and H. Zhao, "Third harmonic generation in graphene and few-layer graphite films," *Phys. Rev. B* **87**, 121406(R) (2013); e-print [arXiv:1301.1042](#).
- ²⁵S. Y. Hong, J. I. Dadap, N. Petrone, P. C. Yeh, J. Hone, and R. M. Osgood, "Optical third-harmonic generation in graphene," *Phys. Rev. X* **3**, 021014 (2013); e-print [arXiv:1301.1697](#).
- ²⁶F. T. Vasko, "Saturation of interband absorption in graphene," *Phys. Rev. B* **82**, 245422 (2010); e-print [arXiv:1010.2392](#).
- ²⁷A. Marini, J. D. Cox, and F. J. García De Abajo, "Theory of graphene saturable absorption," *Phys. Rev. B* **95**, 125408 (2017); e-print [arXiv:1605.06499](#).
- ²⁸G. Xing, H. Guo, X. Zhang, T. C. Sum, and C. H. A. Huan, "The physics of ultrafast saturable absorption in graphene," *Opt. Express* **18**, 4564–4573 (2010).
- ²⁹R. Paschotta and U. Keller, "Passive mode locking with slow saturable absorbers," *Appl. Phys. B: Lasers Opt.* **73**, 653–662 (2001).
- ³⁰Q. Bao, H. Zhang, Y. Wang, Z. Ni, Y. Yan, Z. X. Shen, K. P. Loh, and D. Y. Tang, "Atomic-layer graphene as a saturable absorber for ultrafast pulsed lasers," *Adv. Funct. Mater.* **19**, 3077–3083 (2009); e-print [arXiv:0910.5820](#).
- ³¹Z. Sun, T. Hasan, F. Torrisi, D. Popa, G. Privitera, F. Wang, F. Bonaccorso, D. M. Basko, and A. C. Ferrari, "Graphene mode-locked ultrafast laser," *ACS Nano* **4**, 803–810 (2010); e-print [arXiv:0909.0457](#).
- ³²H. Zhang, D. Tang, R. J. Knize, L. Zhao, Q. Bao, and K. P. Loh, "Graphene mode locked, wavelength-tunable, dissipative soliton fiber laser," *Appl. Phys. Lett.* **96**, 111112 (2010).
- ³³Q. Bao, H. Zhang, Z. Ni, Y. Wang, L. Polavarapu, Z. Shen, Q. H. Xu, D. Tang, and K. P. Loh, "Monolayer graphene as a saturable absorber in a mode-locked laser," *Nano Res.* **4**, 297–307 (2011); e-print [arXiv:1003.0154](#).
- ³⁴I. H. Baek, H. W. Lee, S. Bae, B. H. Hong, Y. H. Ahn, D. I. Yeom, and F. Rotermund, "Efficient mode-locking of sub-70-fs Ti:Sapphire laser by graphene saturable absorber," *Appl. Phys. Express* **5**, 032701 (2012).
- ³⁵Y. Shen, N. C. Harris, S. Skirlo, M. Prabhu, T. Baehr-Jones, M. Hochberg, X. Sun, S. Zhao, H. Larochelle, D. Englund, and M. Soljačić, "Deep learning with coherent nanophotonic circuits," *Nat. Photonics* **11**, 441–446 (2017); e-print [arXiv:1610.02365](#).
- ³⁶H. El Dirani, A. Kamel, M. Casale, S. Kerdiles, C. Monat, X. Letartre, M. Pu, L. K. Oxenløwe, K. Yvind, and C. Sciancalepore, "Annealing-free Si₃N₄ frequency combs for monolithic integration with Si photonics," *Appl. Phys. Lett.* **113**, 081102 (2018).
- ³⁷H. El Dirani, M. Casale, S. Kerdiles, C. Socquet-Clerc, X. Letartre, C. Monat, and C. Sciancalepore, "Crack-free silicon-nitride-on-insulator nonlinear circuits for continuum generation in the C-band," *IEEE Photonics Technol. Lett.* **30**, 355–358 (2018).
- ³⁸M. Bayle, N. Reckinger, J. R. Huntzinger, A. Felten, A. Bakaraki, P. Landois, J. F. Colomer, L. Henrard, A. A. Zahab, J. L. Sauvajol, and M. Paillet, "Dependence of the Raman spectrum characteristics on the number of layers and stacking orientation in few-layer graphene," *Phys. Status Solidi B* **252**, 2375–2379 (2015).
- ³⁹H. A. Hafez, X. Chai, Y. Sekine, M. Takamura, K. Oguri, I. Al-Naib, M. M. Dignam, H. Hibino, and T. Ozaki, "Effects of environmental conditions on the ultrafast carrier dynamics in graphene revealed by terahertz spectroscopy," *Phys. Rev. B* **95**, 165428 (2017).
- ⁴⁰G. P. Agrawal, *Nonlinear Fiber Optics*, 5th ed. (Elsevier, Academic Press: New York, NY, USA, 2013).
- ⁴¹E. Dremetsika, B. Dlubak, S.-P. Gorza, C. Ciret, M.-B. Martin, S. Hofmann, P. Seneor, D. Dolfi, S. Massar, P. Emplit, and P. Kockaert, "Measuring the nonlinear refractive index of graphene using the optical Kerr effect method," *Opt. Lett.* **41**, 3281 (2016); e-print [arXiv:1607.00911](#).
- ⁴²K. Alexander, N. A. Savostianova, S. A. Mikhailov, D. Van Thourhout, and B. Kuyken, "Gate-tunable nonlinear refraction and absorption in graphene-covered silicon nitride waveguides," *ACS Photonics* **12**, 4944–4950 (2018).